

POSTRAINBENCH: A COMPREHENSIVE BENCHMARK AND A NEW MODEL FOR PRECIPITATION FORECASTING

Yujin Tang¹ Jiaming Zhou¹ Xiang Pan² Zeying Gong¹ Junwei Liang^{1,3} *

¹AI Thrust, The Hong Kong University of Science and Technology (Guangzhou)

²School of Atmospheric Science, Nanjing University

³Department of Computer Science and Engineering, The Hong Kong University of Science and Technology
{yujintang, junweiliang}@hkust-gz.edu.cn

ABSTRACT

Accurate precipitation forecasting is a vital challenge of both scientific and societal importance. Data-driven approaches have emerged as a widely used solution for addressing this challenge. However, solely relying on data-driven approaches has limitations in modeling the underlying physics, making accurate predictions difficult. Coupling AI-based post-processing techniques with traditional Numerical Weather Prediction (NWP) methods offers a more effective solution for improving forecasting accuracy. Despite previous post-processing efforts, accurately predicting heavy rainfall remains challenging due to the imbalanced precipitation data across locations and complex relationships between multiple meteorological variables. To address these limitations, we introduce the **PostRainBench**, a comprehensive multi-variable NWP post-processing benchmark consisting of three datasets for NWP post-processing-based precipitation forecasting. We propose **CAMT**, a simple yet effective Channel Attention Enhanced Multi-task Learning framework with a specially designed weighted loss function. Its flexible design allows for easy plug-and-play integration with various backbones. Extensive experimental results on the proposed benchmark show that our method outperforms state-of-the-art methods by 6.3%, 4.7%, and 26.8% in rain CSI on the three datasets respectively. Most notably, our model is the first deep learning-based method to outperform traditional Numerical Weather Prediction (NWP) approaches in extreme precipitation conditions. It shows improvements of 15.6%, 17.4%, and 31.8% over NWP predictions in heavy rain CSI on respective datasets. These results highlight the potential impact of our model in reducing the severe consequences of extreme weather events.

1 INTRODUCTION

Precipitation forecasting (Sønderby et al., 2020; Espeholt et al., 2022) refers to the problem of providing a forecast of the rainfall intensity based on radar echo maps, rain gauge, and other observation data as well as the Numerical Weather Prediction (NWP) models (Shi et al., 2017). Accurate rainfall forecasts can guide people to make optimal decisions in production and life. The frequency and intensity of rainfall varies based on geography. Though the occurrence of extreme precipitation events is relatively infrequent, they can lead to adverse impacts on both agricultural production and community well-being (de Witt et al., 2021).

At present, the most accurate forecasting system is the Numerical Weather Prediction (NWP) method (Bi et al., 2023), which represents atmospheric states as discretized grids and numerically solves partial differential equations that describe the transition between those states. NWP predictions cover a wide range of variables. Each of them provides information about meteorological states (wind speed, temperature, pressure, etc.) and surface states (water vapor on the surface, snow amount, etc.), presenting a multidimensional description of the atmospheric state.

In the past few years, geoscience has begun to use deep learning to better exploit spatial and temporal structures in the data. Studies are beginning to apply combined convolutional–recurrent approaches

*Corresponding author

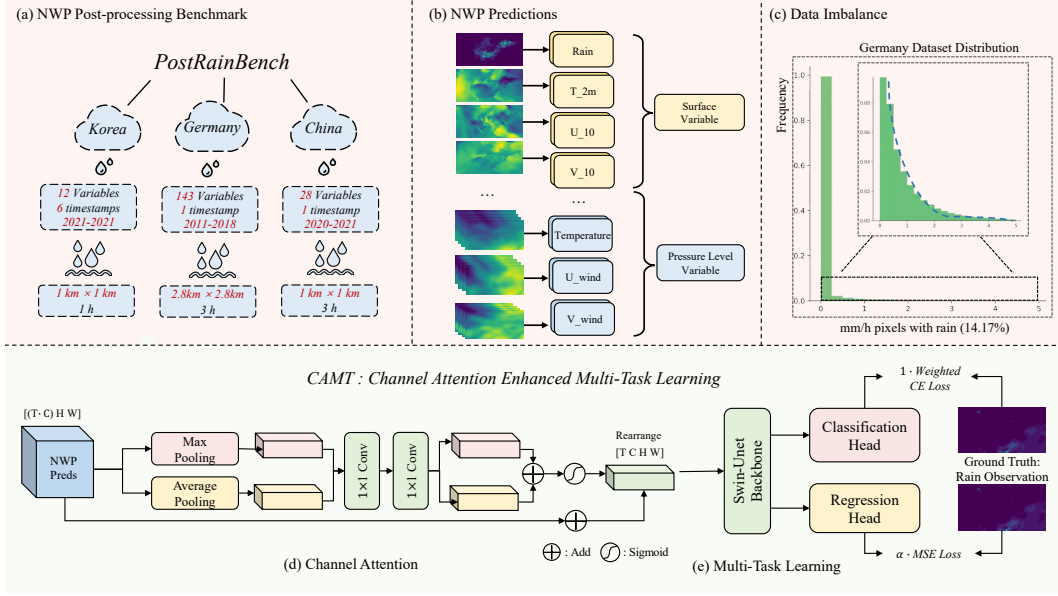


Figure 1: An overview of the proposed **PostRainBench** and **CAMT** framework. (a) illustrates our benchmark’s attributes. (b) shows the input composition. (c) presents the distribution of the German dataset, highlighting the data imbalance challenge. The bottom section illustrates our CAMT workflow: (d) NWP inputs undergo processing by the Channel Attention Module, followed by a Swin-Unet backbone. (e) Multi-task learning with hybrid weighted loss using classification and regression heads.

to geoscientific problems such as precipitation nowcasting (Shi et al., 2015; Wang et al., 2017; Shi et al., 2017). Precipitation nowcasting is mainly based on data-driven extrapolation and lacks physics-based modeling (Kim et al., 2022). Despite continuous efforts to directly enhance global weather forecasting (Lam et al., 2022; Bi et al., 2023; Chen et al., 2023a;b) with deep learning methods, on the NWP side, post-processing methods can be developed to alleviate the predictable biases of NWP models. Combining AI-based and NWP methods can bring about both strengths for a stronger performance (Bi et al., 2023).

For the post-processing task, NWP predictions are fed to a deep learning model which is trained to output refined precipitation forecasts. Rainfall station observations are used as ground truth. In a nutshell, the overall goal is to post-process the predictions from NWP using deep models, under the supervision of rainfall station observations.

However, Post-NWP optimization poses several distinct challenges that distinguish it from typical weather forecasting optimization problems and computer vision tasks.

Variable Selection and Modeling. In NWP, each pixel on the grid has various variables expressing the atmospheric feature state, which exhibit different statistical properties. This discrepancy includes spatial dependence and interdependence among variables, which violate the crucial assumption of identical and independently distributed data (Reichstein et al., 2019). The variables exhibit high correlation among themselves and also possess a degree of noise. Previous approaches have either used all available variables (Rojas-Campos et al., 2022) as input or relied on expert-based variable selection (Kim et al., 2022), which did not fully leverage the modeling capabilities.

Class Imbalance. The distribution of precipitation exhibits a significant imbalance, making model optimization challenging. A prior study (Shi et al., 2017) introduced WMSE, which assigned higher weighting factors to minority classes. Another study (Cao et al., 2022b) combined a reweighting loss with the MSE loss to mitigate the degradation in performance for majority classes. While these approaches have succeeded in improving forecast indicators for the minority class (heavy rainfall), they have inadvertently compromised the model’s performance on the majority class.

Lack of A Unified Benchmark. A previous study, KoMet (Kim et al., 2022), introduced a small dataset covering the time span of two years. Due to the limited data samples, models trained solely on such datasets may risk overfitting to specific data characteristics. Furthermore, KoMet only selected a subset of NWP variables as input. In contrast, another study (Rojas-Campos et al., 2022) utilized all 143 available NWP variables as input. The limited size of the dataset, along with the lack of a standardized method for selecting variables, hinders research progress in improving the NWP post-processing task.

To tackle the aforementioned challenges, we introduce a new model learning framework and a unified benchmark for robust evaluation.

We summarize our contributions as follows:

- We introduce **PostRainBench**, a comprehensive multi-variable benchmark, which covers the full spectrum of scenarios with and without temporal information and various combinations of NWP input variables. This unified benchmark could help accelerate the research area of NWP post-processing-based precipitation forecasting.
- We propose **CAMT**, a simple yet effective Channel Attention Enhanced Multi-task Learning framework with a specially designed weighted loss function. CAMT is flexible and can be plugged into different model backbones.
- On the proposed benchmark, our model outperforms state-of-the-art methods by **6.3%**, **4.7%**, and **26.8%** in rain CSI on three datasets, respectively. Furthermore, it’s worth highlighting a significant milestone achieved by our model. It stands as the first deep learning model to surpass NWP method in heavy rain, with improvements of **15.6%**, **17.4%**, and **31.8%** over NWP predictions across respective datasets. This underscores its potential to effectively mitigate substantial losses in the face of extreme weather events.

2 RELATED WORK

Deep Learning-based Precipitation Nowcasting Regarding precipitation nowcasting as a spatiotemporal sequence forecasting problem, Shi et al. (2015) first proposed Convolutional Long Short-Term Memory (ConvLSTM) to directly predict the future rainfall intensities based on the past radar echo maps. PredRNN (Wang et al., 2017) separated the spatial and temporal memory and communicated them at distinct LSTM levels. Lebedev et al. (2019) used the U-Net architecture (Ronneberger et al., 2015) to nowcast categorical radar images with results that outperformed traditional nowcasting methods. MetNet (Sønderby et al., 2020) employed a combination of a convolutional long short-term memory (LSTM) encoder and an axial attention decoder, which was demonstrated to achieve strong results on short-term low precipitation forecasting using radar data.

NWP Post-processing A recent work (Rojas-Campos et al., 2022) used Conditional Generative Adversarial Network (CGAN) (Goodfellow et al., 2014) to post-process NWP predictions to generate precipitation maps and compared it with U-Net (Ronneberger et al., 2015) and two deconvolution networks. Following the Critical Success Index(CSI) scores, there was an initial high performance in low precipitation forecasting and a progressive decline as the threshold increased, indicating a general difficulty in predicting high precipitation events. NWP’s direct predictions of rain presented the highest scores in predicting high precipitation events over proposed deep learning methods. Another work (Kim et al., 2022) proposed an open dataset with selected NWP predictions as input and compared the performance of three baseline models, U-Net, ConvLSTM and MetNet. The findings were similar, while deep learning models achieved better performance in low rain forecasting, none of the deep learning models surpassed the performance of NWP in heavy rain conditions.

3 POSTRAINBENCH

3.1 TASK FORMULATION

In this study, we consider optimizing the following model:

$$\min_{\mathbf{w}} \left\{ \mathcal{L}(\mathbf{w}; \mathcal{D}) \triangleq \mathbb{E}_{(X_t, y_t) \sim \mathcal{D}} [\ell(y_t; F(X_t, \mathbf{w}))] \right\} \quad (1)$$

where \mathcal{L} is the objective function parameterized by \mathbf{w} on the dataset \mathcal{D} . As shown in Figure 2, the input is NWP predictions X_t , the corresponding ground-truth is rain observation y_t at time t , and ℓ is the loss function between the output of our proposed model $F(\cdot, \mathbf{w})$ and the ground-truth. $X_t = \{\mathbf{x}_{(t-L)}, \mathbf{x}_{(t-L+1)}, \dots, \mathbf{x}_{(t-2)}, \mathbf{x}_{(t-1)}\}$ is a sequence of NWP predictions given by the NWP model at time $t - L - \tau$, where L is the length of the sequence and τ is lead time. Our post-process model $F(\cdot, \mathbf{w})$ takes the sequence of NWP predictions X_t as input, aiming to predict a refined output \tilde{y}_t (at time t), where the rainfall observations y_t (at time t) serve as ground truth to train our model. In our multi-task framework, the prediction of our model at time t is defined as a classification forecast $\tilde{\mathbf{y}}_{cls}$ and a regression forecast $\tilde{\mathbf{y}}_{reg}$. Our proposed model $F(\cdot, \mathbf{w})$ is formulated as:

$$\tilde{\mathbf{y}}_{cls}, \tilde{\mathbf{y}}_{reg} = F(X_t, \mathbf{w}) \quad (2)$$

$$= F(\{\mathbf{x}_{(t-L)}, \mathbf{x}_{(t-L+1)}, \dots, \mathbf{x}_{(t-2)}, \mathbf{x}_{(t-1)}\}, \mathbf{w}) \quad (3)$$

where \mathbf{w} is the trainable parameters. The input X_t , i.e., the sequence of NWP predictions at time t , is organized as $X_t \in \mathbb{R}^{(C*L) \times W \times H}$, where W, H is the width and height of the grid map and C is the number of variables in each pixel. Our model utilizes a classification head and a regression head to generate two final forecasts, $\tilde{\mathbf{y}}_{cls}$ and $\tilde{\mathbf{y}}_{reg}$. $\tilde{\mathbf{y}}_{cls}$ is a probability matrix and each item indicates the probability of class among {'non-rain', 'rain', 'heavy rain'}. $\tilde{\mathbf{y}}_{reg}$ is a prediction value of each pixel in the grid.

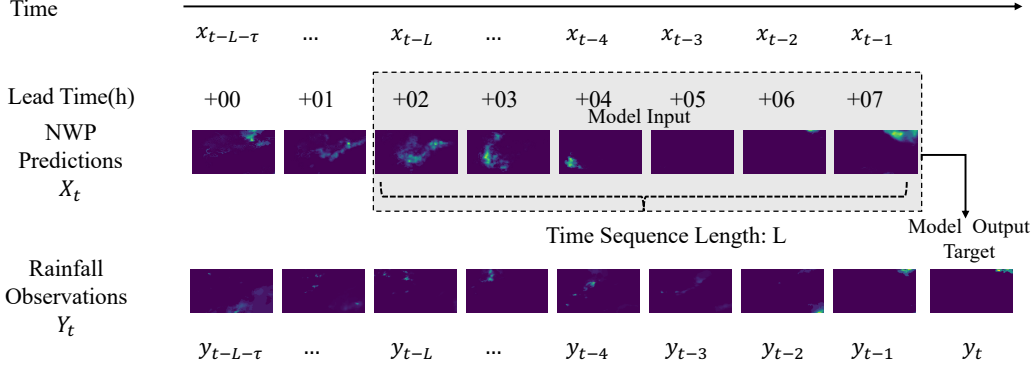


Figure 2: An illustrate of NWP post-processing task. NWP predictions X_t with a time sequence length of L is used as input, while rain observation y_t is used as ground truth.

3.2 EVALUATION METRICS

In terms of evaluation, we adopt commonly used multi-class classification metrics for precipitation forecasting by previous works (Kim et al., 2022). The evaluation metrics are calculated based on the number of true positives (TP_k), false positives (FP_k), true negatives (TN_k), and false negatives (FN_k) for some generic class k . We describe the main metrics we consider as follows:

Critical Success Index (CSI) (Donaldson et al., 1975) is a categorical score that considers more aspects of the confusion matrix similar with F1-score having the value as $\frac{TP_k}{TP_k + FN_k + FP_k}$.

Heidke Skill Score (HSS) (Woo & Wong, 2017) as stated by Hogan et al. (2010), is more equitable in evaluating the forecasting performance. Higher HSS means better performance and a positive HSS indicates that a forecast is better than a random-based forecast. HSS is calculated as $\frac{2 \times (TP_k \times TN_k - FN_k \times FP_k)}{FP_k^2 + TN_k^2 + 2 \times TP_k \times FN_k + (FP_k + TN_k)(TP_k + FP_k)}$.

Please refer to the Section A.6 for all metrics we use in the benchmark.

3.3 DATASETS

To address the issues of limited dataset size and the lack of a standardized criterion for variable selection, we introduce a unified benchmark comprising three datasets. Two of these datasets are

sourced from prior research, while the third is collected from a public challenge. We describe our processing and standardization of the datasets below.

The first dataset, called KoMet (Kim et al., 2022), was collected in South Korea. Its input data is from GDAPS-KIM, a global numerical weather prediction model. GDAPS-KIM provides hourly forecasts for various atmospheric variables. The GDAPS-KIM prediction data is structured as follows: $\mathbf{X} \in \mathbb{R}^{T \times L \times C \times W \times H}$, where each dimension corresponds to the origin time (T) at which the simulation took place, lead time (L) between the origin time and the target prediction time, the variable index (C), and the spatial dimensions of the prediction map (W, H). GDAPS-KIM operates at a spatial resolution of 12 km \times 12 km, resulting in a spatial dimension of 65 \times 50. The variables in GDAPS-KIM can be categorized into two types: pressure level variables and surface variables. For benchmarking purposes, 12 variables out of the 122 are selected according to Korean experts, and we follow this setting in our paper. Detailed descriptions can be found in Table 5.

The second dataset originates from Germany (Rojas-Campos et al., 2022). This dataset covers the period from 2011 to 2018 and is confined to a selected area in West Germany. The input data is derived from the COSMO-DE-EPS forecast (Peralta et al., 2012), which provides 143 variables of the atmospheric state. For this dataset, the forecast with a 3-hour lead time is selected. A detailed description of the COSMO-DE-EPS output can be found in Schättler et al. (2008). The input data has a spatial resolution of 36 \times 36, while the output data is available at a resolution of 72 \times 72. To give a fair comparison between various algorithms, we perform interpolation on both to bring them to a consistent resolution of 64 \times 64.

The third dataset originates from China and provides hourly, 1 km \times 1 km resolution, 3-hour grid point precipitation data for the rainy season. This dataset spans from April to October in both 2020 and 2021. Additionally, it includes 3-hour lead time forecasts from a regional NWP model, with 28 surface and pressure level variables such as 2-meter temperature, 2-meter dew point temperature, 10-meter u and v wind components, and CAPE (Convective Available Potential Energy) values. For all variables provided, please refer to Table 6. Each time frame in this dataset covers a substantial spatial area, featuring a grid size of 430 \times 815. To maintain consistency, we interpolate this dataset to a more manageable 64 \times 64 grid.

We summarize important details of the three datasets in the Table 7.

3.4 DATA DISTRIBUTION

We analyze the distribution of the observed precipitation data, which serves as the ground truth, across the three datasets. In accordance with the framework outlined in Kim et al. (2022), we categorize precipitation into two types: rain and heavy rain, each with its set of evaluation metrics and frame this forecasting problem as a three-class classification task. It is important to note that the threshold for defining heavy rain can vary by location due to differences in rainfall frequency influenced by geographical and climatic factors.

Table 1: Statistics of three datasets.

Dataset	Rain rate (mm/h)	Proportion (%)	Rainfall Level
KoMet	[0.0, 0.1)	87.24	No Rain
	[0.1, 10.0)	11.57	Rain
	[10.0, ∞)	1.19	Heavy Rain
Germany	[0.0, 10^{-5})	85.10	No Rain
	[10^{-5} , 2.0)	13.80	Rain
	[2.0, ∞)	1.10	Heavy Rain
China	[0.0, 0.1)	91.75	No Rain
	[0.1, 2.0)	3.81	Rain
	[2.0, ∞)	4.44	Heavy Rain

In Germany dataset, Rojas-Campos et al. (2022) explores various thresholds including 0.2, 0.5, 1, 2, and 5, we adopt a rain threshold of 10^{-5} mm/h since its distribution is concentrated in [0,1] and we adhere to the rain threshold of 0.1mm/h adopted by Kim et al. (2022) In Korea dataset, we

adhere previous heavy rain threshold of 10mm/h and opt for a unified threshold of 2mm/h in another two datasets, enabling a more equitable comparison. The distribution and the rain categorization of the three datasets are presented in Table 1. It is evident that all three datasets exhibit significant imbalances, which presents a great challenge to predict extreme weather scenarios.

4 METHOD

As illustrated in Figure 1, our model can be divided into three parts. The first part is a channel attention module (Woo et al., 2018). The second part is the Swin-Unet backbone (Cao et al., 2022a) that generates linear projections. The third part is a multi-task learning branch with a hybrid loss. We describe the first and third parts in detail below and put explanations of Swin-Unet in Section A.1 and A.2.

4.1 CHANNEL ATTENTION MODULE

While the data-driven approaches can be improved by incorporating more variables, they also escalate the storage space and memory demands for modeling. Previous approaches either used all available variables as input or relied on expert-driven variable selection, which did not fully harness modeling capabilities.

A recent study (Chen et al., 2023a) viewed the medium-range forecast problem from a multi-modal perspective and used a cross-model transformer to fuse different modalities. It inspires us by emphasizing that the crucial aspect of accurate multi-variable weather forecasting lies in effectively modeling the relationships between different channels (variables).

To this concern, we introduce the Channel Attention Module (CAM), which enables variable selection for a unified NWP post-processing task, and models intricate relationships between variables.

CAM aggregates spatial information of a feature map by using both average-pooling and max-pooling operations, generating two different spatial context descriptors: $\mathbf{F}_{\text{avg}}^c$ and $\mathbf{F}_{\text{max}}^c$. Both descriptors are forwarded to a shared multi-layer perceptron (MLP) to produce a channel attention map $\mathbf{M}_c \in \mathbb{R}^{C \times 1 \times 1}$. To reduce parameter overhead, the hidden activation size is set to $\mathbb{R}^{C/r \times 1 \times 1}$, where r is the reduction ratio. After the shared network, the two output feature vectors are merged with element-wise summation. We employ a residual connection (He et al., 2016) by adding the attention map to the original input, which serves as the input for the subsequent backbone stage.

In short, the channel attention is computed as:

$$\begin{aligned} \mathbf{M}_c(\mathbf{F}) &= \sigma(MLP(AvgPool(\mathbf{F})) + MLP(MaxPool(\mathbf{F}))) \\ &= \sigma(\mathbf{W}_1(\mathbf{W}_0(\mathbf{F}_{\text{avg}}^c)) + \mathbf{W}_1(\mathbf{W}_0(\mathbf{F}_{\text{max}}^c))), \end{aligned} \quad (4)$$

where σ denotes the sigmoid function, $\mathbf{W}_0 \in \mathbb{R}^{C/r \times C}$, and $\mathbf{W}_1 \in \mathbb{R}^{C \times C/r}$. We choose $r = 16$. Note that the MLP weights, \mathbf{W}_0 and \mathbf{W}_1 , are shared for both inputs and the activation function is followed by \mathbf{W}_0 . We choose GeLU activation function instead of ReLU.

The resulting feature maps are then input to the Swin-Unet backbone, as shown in Figure 1.

The backbone model is connected to a classification head and a regression head, which are learned under our proposed multitask learning framework as described in the next section.

4.2 MULTITASK LEARNING WITH HYBRID WEIGHTED LOSS

Prior research has traditionally approached precipitation forecasting as either a regression or classification problem. In practice, people care more about the rain level than specific rain intensity. Considering the realistic needs, a classification task is more appropriate. However, In our practice, we find regression task can enhance the learning for classification task. This approach streamlines model optimization, aligning with the metrics we utilize.

In this paper, we introduce a combination of Mean Squared Error (MSE) loss and weighted Cross-Entropy (CE) loss within a multi-task learning framework, incorporating two task outputs $\tilde{\mathbf{y}}_{cls}, \tilde{\mathbf{y}}_{reg}$ with a hyperparameter α . Utilizing dedicated classification and regression heads encourages the backbone to focus on learning essential features for both tasks.

As previously mentioned, precipitation forecasting grapples with the challenge of highly imbalanced class distributions from a classification standpoint. To tackle this issue, we apply class weights w_c based on the class distribution of each dataset. The full loss function L_{hybrid} is defined as:

$$L_{cls} = \sum_{i=1}^h \sum_{j=1}^w \left(- \sum_{c=1}^M w_c y_t \log(\tilde{y}_{cls}) \right) \quad (5)$$

$$L_{reg} = \sum_{i=1}^h \sum_{j=1}^w (\tilde{y}_{reg} - y_t)^2 \quad (6)$$

$$L_{hybrid} = L_{cls} + \alpha L_{reg} \quad (7)$$

In Equation 5, h and w refer to the spatial resolution, height and width, c refer to the grid’s pixel class, M is the number of classes, and y_t is the ground truth.

5 EXPERIMENTAL EVALUATION

5.1 IMPLEMENTATION DETAILS

We compare our proposed Swin-Unet-based CAMT framework with various strong baselines, including the NWP method, three deep learning models (ConvLSTM, UNet, MetNet). Swin-Unet (Ronneberger et al., 2015) is a Unet-like Transformer. The tokenized image patches are fed into the Swin Transformer-based (Liu et al., 2021) U-shaped Encoder-Decoder architecture with skip connections for local-global semantic feature learning.

The datasets are split into training, validation, and test sets following the configurations outlined in previous studies. For the China dataset, we randomly partition the data into a 6:2:2 ratio. To ensure consistency with prior studies, we select the model with the best CSI performance on the validation set and report its performance on the test set. Each model is run with three different random seeds for robust performance. We use the Adam optimizer for all models.

For the Korea dataset, baseline models are trained with a learning rate of 0.001 (as mentioned in Kim et al. (2022)), while Swin-Unet models are trained with a learning rate of 0.0001. Consistent with previous settings, a batch size of 1 is employed, and all models are trained for 50 epochs. We apply a weight of [1, 5, 30] for the CE Loss. We utilize a hyperparameter α of 100 for the MSE Loss on all datasets. For the Germany dataset, baseline models are trained with a learning rate of 0.001 (as mentioned in Rojas-Campos et al. (2022)), whereas Swin-Unet models are trained with a learning rate of 0.0001. The batch size remains consistent with previous settings at 20, and all models are trained for 30 epochs. We utilize a class weight of [1, 5, 30]. For the China dataset, all models are trained with a learning rate of 10^{-4} for 100 epochs. The weight configuration used is [1, 15, 10].

5.2 RESULTS

As shown in Table 2, for the Korea dataset, our method demonstrates an improvement of 6.3% in rain prediction CSI compared to the state-of-the-art (SOTA) approach, which is ConvLSTM. We highlight that CAMT achieves a remarkable 15.6% improvement in heavy rain prediction CSI over the NWP method, which is the first DL model to surpass NWP results for extreme weather conditions. This result underscores the potential and efficacy of data-driven methods in advancing precipitation forecasting.

For the Germany dataset, U-Net emerges as the top performer among previous models, particularly excelling in rain CSI. Notably, our method achieves a 4.7% improvement over U-Net. When it comes to heavy rain prediction, U-Net’s performance is limited and the NWP model outperforms all previous DL models. Our method shows a substantial 17.4% improvement over NWP, marking a significant advancement.

In the case of the China dataset, the NWP method demonstrates better performance in both rain and heavy rain prediction compared to previous DL models. Our method achieves improvements of 26.8% and 31.8% over the NWP method under these two conditions, respectively. Previous DL

Table 2: Experimental Results on the proposed PostRainBench. Each model undergoes three runs with different random seeds, and we report the mean, standard deviation (std), and best performance in terms of CSI and HSS. The best results are highlighted in **bold**, with the second-best results underlined. We report the relative improvement of our method (Swin-Unet+CAMT) over the best result among the baselines and NWP. In the context of the results, '↑' indicates that higher scores are better.

		Rain				Heavy Rain			
		CSI↑		HSS↑		CSI↑		HSS↑	
		Mean(Std)	Best	Mean(Std)	Best	Mean(Std)	Best	Mean(Std)	Best
Korea	NWP	0.263(±0.000)		*		0.045(±0.000)		*	
	U-Net	0.300(±0.025)	<u>0.322</u>	0.384 (±0.025)	0.408	0.006(±0.005)	0.010	0.011(±0.009)	0.018
	ConvLSTM	<u>0.302</u> (±0.009)	0.312	0.384 (±0.009)	<u>0.395</u>	0.009(±0.007)	<u>0.015</u>	<u>0.016</u> (±0.012)	<u>0.026</u>
	MetNet	0.298(±0.012)	0.307	0.375(±0.014)	0.384	0.005(±0.007)	0.012	0.009(±0.012)	0.023
	Ours	0.321 (±0.005)	0.326	0.384 (±0.007)	0.389	0.052 (±0.010)	0.058	0.089 (±0.017)	0.097
	Ours Δ	+6.3%		+0%		+15.6%		+456.3%	
Germany	NWP	0.338(±0.000)		0.252(±0.000)		<u>0.178</u> (±0.000)		<u>0.173</u> (±0.000)	
	U-Net	<u>0.491</u> (±0.007)	<u>0.495</u>	<u>0.601</u> (±0.006)	<u>0.605</u>	0.082(±0.028)	0.107	0.148(±0.048)	0.189
	ConvLSTM	0.477(±0.026)	0.478	0.587(±0.004)	0.590	0.091(±0.041)	<u>0.121</u>	0.162(±0.068)	<u>0.212</u>
	MetNet	0.485(±0.002)	0.487	0.595(±0.005)	0.599	0.027(±0.016)	0.094	0.147(±0.027)	0.168
	Ours	0.514 (±0.003)	0.518	0.609 (±0.006)	0.616	0.209 (±0.014)	0.224	0.339 (±0.020)	0.359
	Ours Δ	+4.7%		+1.3%		+17.4%		+96.0%	
China	NWP	<u>0.164</u> (±0.000)		<u>0.123</u> (±0.000)		<u>0.110</u> (±0.000)		0.089(±0.000)	
	U-Net	0.065(±0.007)	0.073	0.093(±0.009)	0.103	0.058(±0.014)	0.070	0.089(±0.024)	0.110
	ConvLSTM	0.054(±0.011)	0.066	0.079(±0.009)	0.088	0.065(±0.003)	0.068	<u>0.104</u> (±0.010)	0.114
	MetNet	0.064(±0.019)	<u>0.078</u>	0.061(±0.047)	<u>0.106</u>	0.057(±0.017)	<u>0.076</u>	0.069(±0.057)	<u>0.118</u>
	Ours	0.208 (±0.007)	0.216	0.274 (±0.014)	0.289	0.145 (±0.015)	0.163	0.225 (±0.019)	0.246
	Ours Δ	+26.8%		+122.8%		+31.8%		+116.3%	

* For Korea dataset, NWP method's HSS is not reported. For all NWP method, we only have the mean value.

methods might be struggling with this dataset due to its small sample size, while our method manages to achieve substantial improvements using the proposed CAM and multi-task training framework. This underscores the robustness and versatility of our approach. We make this dataset available and integrate it with the previous two datasets, creating a unified benchmark that could facilitate future research in this field.

5.3 ABLATION STUDY

5.3.1 CAMT COMPONENT

We conduct an ablation study by systematically disabling certain components of our CAMT Component and evaluating the CSI results for both rain and heavy rain in Table 3. Specifically, we focus on the weighted loss, multi-task learning, and channel attention modules as these are unique additions to the Swin-Unet backbone. In the first part, we use Swin-Unet with CAMT framework (a) as a baseline and we disable each component in CAMT and demonstrate their respective outcomes. In the second part, we use Swin-Unet without CAMT framework (e) as a baseline and we gradually add each component to the model to understand its role.

Weighted Loss (b) Without the weighted Loss in CAMT, there is a slight increase in rain CSI, but heavy rain CSI shows a dominant 97.6% decrease. (f) Adding the weighted loss to Swin-Unet results in a 6.0% decrease in rain CSI, but a significant improvement in heavy rain CSI.

Multi-Task Learning (c) Without multi-task learning, there is a 3.7% drop in rain CSI, along with a notable 8.1% decrease in heavy rain CSI. (g) Incorporating multi-task learning into Swin-Unet leads to a comparable performance of rain CSI but brings a slight increase in heavy rain CSI.

CAM (d) In the absence of CAM, we observe a 1.8% decrease in rain CSI and a significant 11.1% decrease in heavy rain CSI. (h) The introduction of CAM into Swin-Unet leads to a rain CSI similar

to the baseline but demonstrates an impressive 11.5% improvement in heavy rain CSI. It indicates that CAM is effective for selecting and modeling multiple weather variables.

Table 3: Ablation study on Germany dataset (Rojas-Campos et al., 2022). We disable components of the framework in each experiment and report rain and heavy rain CSI as the evaluation metric.

	Weighted Loss	Multi-Task Learning	CAM	Rain		Heavy Rain	
				CSI \uparrow	HSS \uparrow	CSI \uparrow	HSS \uparrow
(a)	✓	✓	✓	0.514	0.609	0.209	0.339
(b)	✗	✓	✓	0.517 (+0.6%)	0.625 (+2.6%)	0.042 (-97.6%)	0.008 (-11.1%)
(c)	✓	✗	✓	0.495 (-3.7%)	0.588 (-3.4%)	0.192 (-8.1%)	0.317 (-6.5%)
(d)	✓	✓	✗	0.505 (-1.8%)	0.602 (-1.1%)	0.183 (-11.1%)	0.305 (-11.1%)
(e)	✗	✗	✗	0.521	0.628	0.000	0.000
(f)	✓	✗	✗	0.490 (-6.0%)	0.580 (-7.6%)	0.188 $\uparrow\uparrow\uparrow$	0.307 $\uparrow\uparrow\uparrow$
(g)	✗	✓	✗	0.516 (-0.1%)	0.629 (+0.2%)	0.067 \uparrow	0.007 \uparrow
(h)	✗	✗	✓	0.513 (-1.5%)	0.624 (-0.6%)	0.115 $\uparrow\uparrow$	0.204 $\uparrow\uparrow$

Although Swin-UNet can achieve a relatively high CSI when used alone (e), it does not have the ability to predict heavy rain. Importantly, these three enhancements complement each other. Weighted loss and multi-task learning are effective in improving simultaneous forecasting under the unbalanced distribution of light rain and heavy rain, while CAM provides comprehensive improvements.

5.3.2 ABLATION ON BACKBONE

We conduct another ablation study by replacing Swin-UNet backbone with ViT (Dosovitskiy et al., 2020) backbone under our CAMT framework in Table 4.

For the Korea dataset, ViT outperforms Swin-UNet in rain CSI and HSS but shows a slight decrease in heavy rain CSI. Importantly, its performance remains higher than that of NWP, which shows the effectiveness of CAMT. For the Germany dataset, though its performance on rain CSI is limited, the ViT model still demonstrates a remarkable performance in heavy rain CSI and surpasses NWP. For the China dataset, ViT outperforms all baseline models and is only second to Swin-UNet.

Table 4: Ablation study with ViT backbone, we highlight the best results in **bold**.

		Rain				Heavy Rain			
		CSI \uparrow		HSS \uparrow		CSI \uparrow		HSS \uparrow	
		Mean(Std)	Best	Mean(Std)	Best	Mean(Std)	Best	Mean(Std)	Best
Korea	ViT+CAMT	0.326 (± 0.004)	0.329	0.394 (± 0.001)	0.395	0.049 (± 0.010)	0.055	0.083 (± 0.017)	0.097
	Swin-UNet+CAMT	0.321 (± 0.005)	0.326	0.384 (± 0.007)	0.389	0.052 (± 0.010)	0.058	0.089 (± 0.017)	0.097
Germany	ViT+CAMT	0.484 (± 0.004)	0.488	0.576 (± 0.005)	0.581	0.194 (± 0.023)	0.041	0.050 (± 0.043)	0.078
	Swin-UNet+CAMT	0.514 (± 0.003)	0.518	0.609 (± 0.006)	0.616	0.209 (± 0.014)	0.224	0.339 (± 0.020)	0.359
China	ViT+CAMT	0.177 (± 0.004)	0.181	0.217 (± 0.006)	0.224	0.068 (± 0.033)	0.105	0.091 (± 0.052)	0.149
	Swin-UNet+CAMT	0.208 (± 0.007)	0.216	0.274 (± 0.014)	0.289	0.145 (± 0.015)	0.163	0.225 (± 0.019)	0.246

These experiments highlight the potential of the ViT model. We also conduct experiments with three baseline models but observe limited improvements. We believe that addressing the challenge of imbalanced precipitation forecasting requires a more robust backbone and the use of our CAMT framework, which incorporates multi-task information to enrich the learning process of this task.

6 CONCLUSION

In this paper, we introduce **PostRainBench**, a comprehensive multi-variable benchmark for NWP post-processing-based precipitation forecasting and we present **CAMT**, Channel Attention Enhanced Multi-task Learning framework with a specially designed weighted loss function. Our approach demonstrates outstanding performance improvements compared to the three baseline models and the NWP method. In conclusion, our research provides novel insights into the challenging do-

main of highly imbalanced precipitation forecasting tasks. We believe our benchmark could help advance the model development of the research community.

Reproducibility Statement We provide the details of implementing our method as well as instructions to reproduce the experiments in Section 5. The datasets we used are publicly available. We will release the source code upon acceptance.

REFERENCES

- Lindsey R Barnes, David M Schultz, Eve C Grunfest, Mary H Hayden, and Charles C Benight. Corrigendum: False alarm rate or false alarm ratio? *Weather and Forecasting*, 24(5):1452–1454, 2009.
- Kaifeng Bi, Lingxi Xie, Hengheng Zhang, Xin Chen, Xiaotao Gu, and Qi Tian. Accurate medium-range global weather forecasting with 3d neural networks. *Nature*, pp. 1–6, 2023.
- Hu Cao, Yueyue Wang, Joy Chen, Dongsheng Jiang, Xiaopeng Zhang, Qi Tian, and Manning Wang. Swin-unet: Unet-like pure transformer for medical image segmentation. In *European conference on computer vision*, pp. 205–218. Springer, 2022a.
- Yuan Cao, Lei Chen, Danchen Zhang, Leiming Ma, and Hongming Shan. Hybrid weighting loss for precipitation nowcasting from radar images. In *ICASSP 2022-2022 IEEE International Conference on Acoustics, Speech and Signal Processing (ICASSP)*, pp. 3738–3742. IEEE, 2022b.
- Kang Chen, Tao Han, Junchao Gong, Lei Bai, Fenghua Ling, Jing-Jia Luo, Xi Chen, Leiming Ma, Tianning Zhang, Rui Su, et al. Fengwu: Pushing the skillful global medium-range weather forecast beyond 10 days lead. *arXiv preprint arXiv:2304.02948*, 2023a.
- Lei Chen, Xiaohui Zhong, Feng Zhang, Yuan Cheng, Yinghui Xu, Yuan Qi, and Hao Li. Fuxi: A cascade machine learning forecasting system for 15-day global weather forecast. *arXiv preprint arXiv:2306.12873*, 2023b.
- Christian Schroeder de Witt, Catherine Tong, Valentina Zantedeschi, Daniele De Martini, Alfredo Kalaitzis, Matthew Chantry, Duncan Watson-Parris, and Piotr Bilinski. Rainbench: Towards data-driven global precipitation forecasting from satellite imagery. In *Proceedings of the AAAI Conference on Artificial Intelligence*, volume 35, pp. 14902–14910, 2021.
- RJ Donaldson, Rosemary M Dyer, and Michael J Kraus. Objective evaluator of techniques for predicting severe weather events. In *Bulletin of the American Meteorological Society*, volume 56, pp. 755–755. AMER METEOROLOGICAL SOC 45 BEACON ST, BOSTON, MA 02108-3693, 1975.
- Alexey Dosovitskiy, Lucas Beyer, Alexander Kolesnikov, Dirk Weissenborn, Xiaohua Zhai, Thomas Unterthiner, Mostafa Dehghani, Matthias Minderer, Georg Heigold, Sylvain Gelly, et al. An image is worth 16x16 words: Transformers for image recognition at scale. *arXiv preprint arXiv:2010.11929*, 2020.
- Lasse Espeholt, Shreya Agrawal, Casper S nderby, Manoj Kumar, Jonathan Heek, Carla Bromberg, Cenk Gizen, Rob Carver, Marcin Andrychowicz, Jason Hickey, et al. Deep learning for twelve hour precipitation forecasts. *Nature communications*, 13(1):1–10, 2022.
- Ian Goodfellow, Jean Pouget-Abadie, Mehdi Mirza, Bing Xu, David Warde-Farley, Sherjil Ozair, Aaron Courville, and Yoshua Bengio. Generative adversarial nets. *Advances in neural information processing systems*, 27, 2014.
- Kaiming He, Xiangyu Zhang, Shaoqing Ren, and Jian Sun. Deep residual learning for image recognition. In *Proceedings of the IEEE conference on computer vision and pattern recognition*, pp. 770–778, 2016.
- Robin J Hogan, Christopher AT Ferro, Ian T Jolliffe, and David B Stephenson. Equitability revisited: Why the “equitable threat score” is not equitable. *Weather and Forecasting*, 25(2):710–726, 2010.
- Taehyeon Kim, Namgyu Ho, Donggyu Kim, and Se-Young Yun. Benchmark dataset for precipitation forecasting by post-processing the numerical weather prediction. *arXiv preprint arXiv:2206.15241*, 2022.

- Remi Lam, Alvaro Sanchez-Gonzalez, Matthew Willson, Peter Wirsberger, Meire Fortunato, Alexander Pritzel, Suman Ravuri, Timo Ewalds, Ferran Alet, Zach Eaton-Rosen, et al. Graphcast: Learning skillful medium-range global weather forecasting. *arXiv preprint arXiv:2212.12794*, 2022.
- Vadim Lebedev, Vladimir Ivashkin, Irina Rudenko, Alexander Ganshin, Alexander Molchanov, Sergey Ovcharenko, Ruslan Grokhovetskiy, Ivan Bushmarinov, and Dmitry Solomentsev. Precipitation nowcasting with satellite imagery. In *Proceedings of the 25th ACM SIGKDD international conference on knowledge discovery & data mining*, pp. 2680–2688, 2019.
- Ze Liu, Yutong Lin, Yue Cao, Han Hu, Yixuan Wei, Zheng Zhang, Stephen Lin, and Baining Guo. Swin transformer: Hierarchical vision transformer using shifted windows. In *Proceedings of the IEEE/CVF international conference on computer vision*, pp. 10012–10022, 2021.
- C Peralta, Z Ben Bouallègue, SE Theis, C Gebhardt, and M Buchhold. Accounting for initial condition uncertainties in cosmo-de-eps. *Journal of Geophysical Research: Atmospheres*, 117 (D7), 2012.
- Markus Reichstein, Gustau Camps-Valls, Bjorn Stevens, Martin Jung, Joachim Denzler, Nuno Carvalho, and fmm Prabhat. Deep learning and process understanding for data-driven earth system science. *Nature*, 566(7743):195–204, 2019.
- Adrian Rojas-Campos, Michael Langguth, Martin Wittenbrink, and Gordon Pipa. Deep learning models for generation of precipitation maps based on numerical weather prediction. *EGU sphere*, pp. 1–20, 2022.
- Olaf Ronneberger, Philipp Fischer, and Thomas Brox. U-net: Convolutional networks for biomedical image segmentation. In *Medical Image Computing and Computer-Assisted Intervention—MICCAI 2015: 18th International Conference, Munich, Germany, October 5-9, 2015, Proceedings, Part III 18*, pp. 234–241. Springer, 2015.
- U Schättler, G Doms, and C Schraff. A description of the nonhydrostatic regional cosmo-model part vii: user’s guide. *Deutscher Wetterdienst Rep. COSMO-Model*, 4:142, 2008.
- Xingjian Shi, Zhourong Chen, Hao Wang, Dit-Yan Yeung, Wai-Kin Wong, and Wang-chun Woo. Convolutional lstm network: A machine learning approach for precipitation nowcasting. *Advances in neural information processing systems*, 28, 2015.
- Xingjian Shi, Zhihan Gao, Leonard Lausen, Hao Wang, Dit-Yan Yeung, Wai-kin Wong, and Wang-chun Woo. Deep learning for precipitation nowcasting: A benchmark and a new model. *Advances in neural information processing systems*, 30, 2017.
- Casper Kaae Sønderby, Lasse Espeholt, Jonathan Heek, Mostafa Dehghani, Avital Oliver, Tim Salmans, Shreya Agrawal, Jason Hickey, and Nal Kalchbrenner. Metnet: A neural weather model for precipitation forecasting. *arXiv preprint arXiv:2003.12140*, 2020.
- Michail Tarasiou, Erik Chavez, and Stefanos Zafeiriou. Vits for sits: Vision transformers for satellite image time series. In *Proceedings of the IEEE/CVF Conference on Computer Vision and Pattern Recognition*, pp. 10418–10428, 2023.
- Yunbo Wang, Mingsheng Long, Jianmin Wang, Zhifeng Gao, and Philip S Yu. Predrnn: Recurrent neural networks for predictive learning using spatiotemporal lstms. *Advances in neural information processing systems*, 30, 2017.
- Sanghyun Woo, Jongchan Park, Joon-Young Lee, and In So Kweon. Cbam: Convolutional block attention module. In *Proceedings of the European conference on computer vision (ECCV)*, pp. 3–19, 2018.
- Wang-chun Woo and Wai-kin Wong. Operational application of optical flow techniques to radar-based rainfall nowcasting. *Atmosphere*, 8(3):48, 2017.

A APPENDIX

A.1 BACKBONES

U-Net (Ronneberger et al., 2015) is a model designed to solve the image segmentation problem in biomedical images. During the propagation of the encoder part, important features are captured in a low-dimensional form.

ConvLSTM (Shi et al., 2015; 2017) is a model that combines LSTM and convolutional operations, each designed to model temporal and spatial relationships, respectively, within sequences of images.

MetNet (Sønderby et al., 2020) employs a spatial downsampler for input size reduction via convolutional layers. The temporal encoder utilizes the ConvLSTM structure to capture spatial-temporal data per pixel. The feature map then undergoes self-attention in the Spatial Aggregator for global context integration before passing through a classifier to output precipitation probabilities for each pixel.

Swin-Unet (Cao et al., 2022a) is a Unet-like Transformer. The tokenized image patches are fed into the Swin Transformer-based U-shaped Encoder-Decoder architecture with skip connections for local-global semantic feature learning. Specifically, it uses hierarchical Swin Transformer (Liu et al., 2021) with shifted windows as the encoder and decoder.

ViT (Dosovitskiy et al., 2020) apply a pure Transformer architecture on image data, by proposing a simple, yet efficient image tokenization strategy. We follow previous work (Tarasiou et al., 2023) to employ Transformers for dense prediction.

A.2 SWIN-UNET ARCHITECTURE

The overall architecture of Swin-Unet is presented in Figure 3. Swin-Unet consists of encoder, bottleneck, decoder and skip connections. The basic unit of Swin-Unet is Swin Transformer block.

For the encoder, the input images are split into non-overlapping patches with patch size of 4×4 . Furthermore, a linear embedding layer is applied to projected feature dimension into arbitrary dimension (represented as C). The transformed patch tokens pass through several Swin Transformer blocks and patch merging layers to generate the hierarchical feature representations. Specifically, patch merging layer is responsible for downsampling and increasing dimension, and Swin Transformer block is responsible for feature representation learning.

The decoder is composed of Swin Transformer block and patch expanding layer. The extracted context features are fused with multiscale features from encoder via skip connections to complement the loss of spatial information caused by down-sampling. In contrast to patch merging layer, a patch expanding layer is specially designed to perform up-sampling. The patch expanding layer reshapes feature maps of adjacent dimensions into a large feature maps with $2\times$ up-sampling of resolution.

In the end, the last patch expanding layer is used to perform $4\times$ up-sampling to restore the resolution of the feature maps to the input resolution ($W \times H$). In our multi-task framework, two linear projection layers are applied on these up-sampled features to output the pixel-level classification and regression predictions.

A.3 KOREA DATASET VARIABLE

A.4 CHINA DATASET VARIABLE

A.5 POSTRAINBENCH DATASET SUMMARY

A.6 EXPERIMENT RESULTS WITH MORE METRICS

We report more evaluation metrics of all models. The evaluation metrics are calculated based on the number of true positives (TP_k), false positives (FP_k), true negatives (TN_k), and false negatives (FN_k) for some generic class k as follows:

Table 5: List of variables contained in the Korea dataset. Pressure level variables contain atmospheric features at different pressure levels, and surface variables contain some other features as well as those in Pressure level variables but do not at certain pressure levels. † indicates the variable with integer type.

Type	Long name	Short name	Description	Unit
Pressure Level	U-component of wind	u	Wind in x/longitude-direction	(ms^{-1})
	V-component of wind	v	Wind in y/latitude direction	(ms^{-1})
	Temperature	T	Temperature	(K)
	Relative humidity	rh liq	Humidity relative to saturation	(%)
	Geopotential	hgt	Proportional to the height of a pressure level	($m^2 s^{-2}$)
Surface	Rain	rain	Rain	(mm/h)
	Snow	snow	Snow	(cm/h)
	Height of PBL	hpbl	Height of planetary boundary layer	(km)
	Type of PBL [†]	pbtype	Type of planetary boundary layer	-
	2m specific humidity	q2m	Specific humidity at 2m height	(g/kg)
	2m relative humidity	rh2m	Humidity relative to saturation at 2m height	(%)
	2m temperature	t2m	Temperature at 2m height above surface	(K)
	Surface temperature	tsfc	Surface temperature	(K)
	10m u component of wind	u10m	Wind in x/longitude-direction at 10m height	(ms^{-1})
	10m v component of wind	v10m	Wind in y/latitude-direction at 10m height	(ms^{-1})
	Topography	topo	Topography	(m)
Pressure of surface	ps	Pressure of surface	(Pa)	

Table 6: List of variables contained in the China dataset. Pressure level variables contain atmospheric features at different pressure levels, and surface variables contain some other features as well as those in Pressure level variables but do not at certain pressure levels.

Type	Long name	Short name	Level	Unit
Pressure Level	U-component of wind	u	200,500,700,850,925	(ms^{-1})
	V-component of wind	v	200,500,700,850,925	(ms^{-1})
	Temperature	T	500,700,850,925	(K)
	Relative humidity	rh liq	500,700,850,925	(%)
Surface	Rain	rain	*	(mm/h)
	Convective Rain	rain_thud	*	(mm/h)
	Large-scale Rain	rain_big	*	(mm/h)
	Convective Available Potential Energy [†]	cape	*	(J/kg)
	Precipitable Water	PWAT	*	(kg/m^2)
	Mean Sea Level	msl	*	(hPa)
	2m temperature	t2m	*	($^{\circ}C$)
	2m dew point temperature	d2m	*	($^{\circ}C$)
	10m component of wind	u10m	*	(ms^{-1})
10m v component of wind	v10m	*	(ms^{-1})	

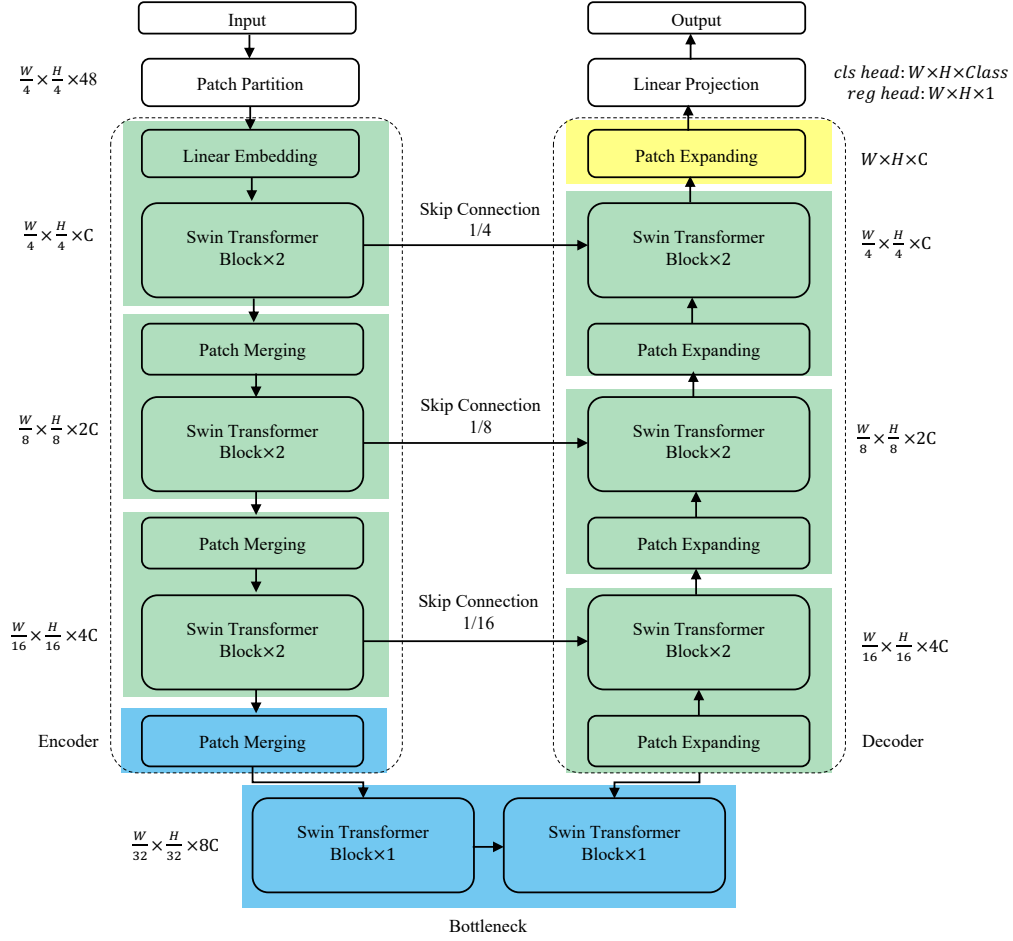


Figure 3: The architecture of Swin-Unet, which is composed of encoder, bottleneck, decoder and skip connections. Encoder, bottleneck and decoder are all constructed based on swin transformer block.

Table 7: Comparison of three NWP datasets with different spatial and temporal resolutions.

Dataset	Korea	Germany	China
Variable type	Pressure Level and Surface		
Variable numbers	12	143	28
Time period	2020-2021	2011-2018	2020-2021
Spatial resolution	12km \times 12km	2.8km \times 2.8km	1km \times 1km
Temporal resolution	1h	3h	3h
Temporal Window Size	6	1	1
Data shape (T C H W)	(6, 12, 50, 65)	(1, 143, 64, 64)	(1, 28, 64, 64)
Data split [train val test]	[4920, 2624, 2542]	[15189, 2725, 2671]	[2264, 752, 760]
Data size	47.9GB	16.2GB	3.6GB

- **Critical Success Index (CSI)** (Donaldson et al., 1975) is a categorical score that considers more aspects of the confusion matrix similar with F1-score having the value as

$$\frac{TP_k}{TP_k + FN_k + FP_k}$$

- **Heidke Skill Score (HSS)** (Woo & Wong, 2017) as stated by (Hogan et al., 2010), is more equitable in evaluating the forecasting performance. Higher HSS means better performance

and a positive HSS indicates that a forecast is better than a random-based forecast. HSS is calculated as $\frac{2 \times (TP_k \times TN_k - FN_k \times FP_k)}{FP_k^2 + TN_k^2 + 2 \times TP_k \times FN_k + (FP_k + TN_k)(TP_k + FN_k)}$.

- **Accuracy (ACC)** returns an overall measure of how much the model is correctly predicting on the entire set of data.
- **Probability of Detection (POD)** is a recall calculated as $\frac{TP_k}{TP_k + FP_k}$.
- **False Alarm Ratio (FAR)** (Barnes et al., 2009) is the number of false alarms per the total number of warnings or alarms, also known as the probability of false detection. It is computed as $\frac{FN_k}{TP_k + FN_k}$.
- **Bias** is defined as the ratio of the observed frequency of occurrence of a phenomenon to the frequency of the occurrence predicted by the forecast model. $\frac{TP_k + FP_k}{TP_k + FN_k}$. If it has a value greater than 1, it means that the frequency of occurrence predicted by the forecasting model is greater than the frequency of occurrence of the actual phenomenon, and therefore more frequent prediction is made. The more accurate the forecast, the closer this index is to 1.

Table 8: Evaluation metrics on three datasets. Best performances are marked in **bold**. ‘↑’ indicates that higher scores are better, ‘↓’ indicates that higher scores are worse.

		Rain						Heavy Rain					
		Acc↑	POD↑	CSI↑	FAR↓	Bias	HSS↑	Acc↑	POD↑	CSI↑	FAR↓	Bias	HSS↑
Korea	NWP	0.747	0.633	0.263	0.690	2.042	*	0.985	0.055	0.045	0.795	0.266	*
	U-Net	0.860	0.430	0.305	0.489	0.841	0.387	0.987	0.001	0.001	0.750	0.002	0.001
	ConvLSTM	0.860	0.446	0.312	0.492	0.878	0.395	0.986	0.011	0.010	0.874	0.083	0.018
	MetNet	0.853	0.457	0.307	0.517	0.946	0.384	0.987	0.013	0.012	0.805	0.067	0.023
	Ours	0.832	0.559	0.322	0.569	1.299	0.388	0.979	0.067	0.048	0.908	0.729	0.068
Germany	NWP	0.728	0.925	0.338	0.652	2.657	0.252	0.980	0.434	0.178	0.767	1.863	0.173
	U-Net	0.903	0.631	0.495	0.305	0.908	0.605	0.990	0.053	0.051	0.412	0.090	0.095
	ConvLSTM	0.896	0.623	0.475	0.334	0.935	0.583	0.990	0.048	0.045	0.566	0.111	0.085
	MetNet	0.895	0.653	0.483	0.349	1.003	0.590	0.990	0.000	0.000	0.694	0.001	0.001
	Ours	0.884	0.811	0.513	0.418	1.393	0.610	0.989	0.280	0.207	0.557	0.632	0.338
China	NWP	0.843	0.433	0.164	0.792	2.082	0.123	0.903	0.348	0.110	0.861	2.512	0.089
	U-Net	0.914	0.071	0.060	0.725	0.261	0.084	0.950	0.053	0.042	0.821	0.294	0.064
	ConvLSTM	0.909	0.083	0.066	0.756	0.339	0.088	0.941	0.099	0.066	0.837	0.607	0.094
	MetNet	0.915	0.086	0.072	0.680	0.268	0.106	0.947	0.104	0.076	0.778	0.466	0.118
	Ours	0.873	0.454	0.216	0.708	1.553	0.289	0.943	0.210	0.135	0.727	0.768	0.209

For accuracy (Acc), our model performs lower than the baseline deep learning models but higher than NWP. However, it’s important to note that accuracy may not provide realistic insights in an extremely imbalanced case. If the model predicts all instances as no-rain, it could achieve a better score. For probability of detection (Pod), our model ranks second only to NWP and outperforms all deep learning models. In terms of critical success index (CSI) and Heidke skill score (HSS), our model consistently outperforms the baseline models, as discussed earlier. The false alarm ratio (Far) measures whether the forecasting model predicts an event more frequently than it actually occurs. Our model exhibits higher but acceptable values in the rain category compared to other deep-learning models, reflecting the trade-off between enhanced forecasting ability and overforecast. In the heavy rain category, our model’s bias is less than 1 and closer to 1, indicating a more accurate forecast.